Suppression of shocked-bubble expansion due to tissue confinement with application to shock-wave lithotripsy

Jonathan B. Freund[a)]
Mechanical Science and Engineering and Aerospace Engineering, University of Illinois at Urbana-Champaign, 1206 West Green Street MC-244, Urbana, Illinois 61801, USA

(Received 12 October 2007; revised 29 February 2008; accepted 29 February 2008)

Estimates are made of the effect of tissue confinement on the response of small bubbles subjected to lithotriptor shock pressures. To do this the Rayleigh–Plesset equation, which governs the dynamics of spherical bubbles, is generalized to treat a bubble in a liquid region (blood), which is in turn encased within an elastic membrane (like a vessel's basement membrane), beyond which a Voigt viscoelastic material models the exterior tissue. Material properties are estimated from a range of measurements available for kidneys and similar soft tissues. Special attention is given to the constitutive modeling of the basement membranes because of their expected importance due to their proximity to the bubble and their toughness. It is found that the highest expected values for the elasticity of the membrane and surrounding tissue are insufficient to suppress bubble growth. The reduced confinement of a cylindrical vessel should not alter this conclusion. Tissue viscosities taken from ultrasound measurements suppress bubble growth somewhat, though not to a degree expected to resist injury. However, the higher reported viscosities measured by other means, which are arguably more relevant to the deformations caused by growing bubbles, do indeed significantly suppress bubble expansion. © *2008 Acoustical Society of America.* [DOI: 10.1121/1.2902171]

PACS number(s): 43.80.Gx, 43.35.Wa, 43.40.Ng [ROC] Pages: 2867–2874

I. INTRODUCTION

There is strong evidence that inertial cavitation causes much of the injury to renal tissue that can accompany the treatment of kidney stones with shock-wave lithotripsy (e.g., Bailey *et al.*[1]). However, the detailed mechanisms of how a growing and collapsing cavitation bubble interacts with the tissue to cause injury are not understood. It is curious, for example, that ~1000 shocks are required before significant injuries are observed.[2] (A typical treatment delivers ~2000 shocks.) It can be speculated that this delay might be due to the scarcity of cavitation nuclei, and that some other mechanism such as shear[3,4] initiates injury. Artificially adding cavitation nuclei has been shown to increase injury,[5] but it remains unclear what happens under normal physiological conditions. In this paper, we develop and parametrize a simple model to assess whether or not the confinement afforded by the renal structures where injury is observed might play a role in suppressing cavitation. The main question we ask with the model is what tissue mechanical properties are needed to suppress damaging bubble expansion: is the tissue expected to be weak or strong as far as an expanding cavitation bubble is concerned? Mechanical properties from several types of experiments on kidneys and other soft tissues are considered.

The possibility that expanding bubbles rupture renal blood vessels was analyzed in some detail by Zhong *et al.*[6,7] They showed that confinement, either by tissue[6] or in blood vessel phantoms,[7] reduces time to bubble collapse and therefore presumably also the size and potential for injury of the expanding cavitation bubbles. However, the phantom vessels they used were significantly larger than most of the blood vessels in kidney tissue, especially in the medulla toward the papilla tip where damage is first observed,[8] and their elasticity relative to that expected for renal vessels and tubules was not characterized. Nevertheless, the experiments clearly showed that only a few shocks were necessary to rupture them via expanding cavitation bubbles. Zhong *et al.*[7] used arguments based on the energetics of expanding bubbles at the critical radius—the radius at which they would encounter the inner vessel wall—to suggest that smaller vessels would be even more susceptible to this mechanism. This approach assumes that the elastic confinement of the vessel is not coupled to the dynamics of the bubble. We account for this in this paper. The opposite extreme would be to study bubble dynamics with completely rigid confinement, such as recently done by Cui *et al.*,[9] who studied the dynamics of spherical bubbles between parallel rigid walls. In this case, of course, it is not possible to tell if actual tissue would be strained to the point of tearing.

The Rayleigh–Plesset equation and related spherical bubble models have been extended to treat bubbles in viscoelastic material[10–12] or bubbles in liquids surrounded by viscoelastic material.[13] These show, as expected, that sufficient elastic resistance suppresses bubble growth and subsequent dynamics. We generalize this approach to a configuration that accounts for more microscopic features of kidney tissue: the bubble is in a liquid bounded by an elastic membrane beyond which is viscoelastic tissue. We do this for a simple geometry, our main objective being to couple viscoelastic properties, as estimated from experimental measurements of kidney and similar tissues, with bubble dynamics. As seen in Fig. 1, the basic geometry is indeed crude. It is a spherical gas bubble in a concentric liquid-filled spheri-

a)Electronic mail: jbfreund@uiuc.edu.

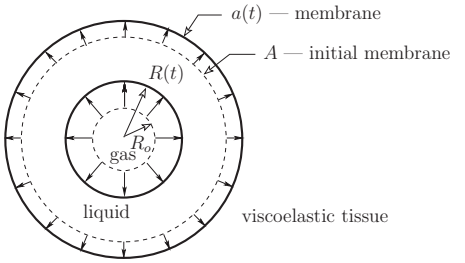

FIG. 1. Model geometry schematic. A bubble radius $r(t)$ [initially $r(0)=R_0$] is positioned at the center of an elastic membrane radius $a(t)$ [initially $a(0)=A$]. The elastic membrane is surrounded by a Voigt viscoelastic material that models tissue.

cal elastic membrane, the tissue beyond which is viscoelastic. The membrane dynamics are coupled with the bubble, liquid, and viscoelastic region dynamics in Sec. II for a model lithotriptor shock pressure history (Sec. II B). Constitutive models and estimates of properties are developed in Sec. III.

Clearly this model was selected for its geometric simplicity and is only a crude model of the geometry of the blood vessels in the kidney, which are approximately cylindrical. However, if spherical confinement is estimated to be unsuccessful in restricting the expansion of the bubble, it is not expected that the weaker confinement afforded by a cylindrical vessel would be more significant. In this sense, we are establishing an upper bound on confinement. If the bubble does not "feel" the confinement in this artificial sphere case, it is even less likely to do so in a cylindrical geometry, where flow along the cylindrical tubule or vessel would facilitate release of the pressure. We shall see in Sec. IV that this is indeed the case for upper estimates on the confinement afforded by elasticity. Further justification of this perspective is provided in the appendix via estimates of the time scales for pressure release by flow along the vessel in both inertia- and viscosity-dominated limits. Both mechanisms are estimated to be too slow to fundamentally change the confinement. The detailed simulations of Ye and Bull[14] show how deformations of an arteriole wall in an embolotherapy application significantly reduce the pressure environment of a confined bubble relative to a rigid wall.[15] This also supports our neglect of flow along the vessel as a pressure release mechanism in making our estimates.

II. BUBBLE DYNAMICS

A. Generalization of the Rayleigh–Plesset equation

Adding the effect of the concentric membrane and exterior viscoelastic material shown in Fig. 1 to the Rayleigh–Plesset equation is straightforward, constituting only a minor change to its derivation. As usual, we neglect any dynamics of the gas phase in the bubble. Under the conditions of interest in shock-wave lithotripsy, the inertia and viscosity of the gas will be negligible relative to that of the liquid except perhaps at collapse, which is not considered in detail in this study. Spherical symmetry and our assumption of an incompressible medium dictate that the radial velocity has the form

$$u(r,t)=\frac{F(t)}{r^2}, \tag{1}$$

where r is the radial coordinate. At the bubble surface $[r=R(t)]$, the fluid velocity must match the bubble surface velocity $[u(R,t)=R]$, which gives $F(t)=R^2\dot{R}$, where the overset dot indicates a time derivative. The appropriate incompressible-medium momentum equation in spherical coordinates is[16]

$$\rho\left(\frac{\partial u}{\partial t}+u\frac{\partial u}{\partial r}\right)=-\frac{\partial p}{\partial r}+\frac{\partial \tau_{rr}}{\partial r}+\frac{3\tau_{rr}}{r}, \tag{2}$$

where p is the pressure, ρ is the density, and τ_{rr} is the radial-normal deviatoric stress. As assumed recently by Yang and Church[12] for a bubble directly in a viscoelastic material, we employ a Voigt model for the viscoelasticity,

$$\tau_{rr}=2(G\gamma+\mu_t\dot{\gamma}). \tag{3}$$

Here, G is the shear modulus of the medium, which for an incompressible medium is one-third the Young's modulus, and μ_t is its viscosity. The simple combination of elastic and viscous effects in the Voigt model is appropriate given the level of detail available in experimental measurements of tissue properties. In Eq. (3), γ is the strain and $\dot{\gamma}$ is the rate of strain,

$$\dot{\gamma}=\frac{\partial u}{\partial r}. \tag{4}$$

Applying Eq. (1) to Eq. (4) gives

$$\dot{\gamma}=-\frac{2R^2\dot{R}}{r^3}, \tag{5}$$

and the corresponding strain from the reference condition (for which $R=R_0$) is thus

$$\gamma=-\frac{2}{3r^3}(R^3-R_0^3). \tag{6}$$

The standard next step in the derivation of the Rayleigh–Plesset equation is an integration of Eq. (2) from $r-R(t)$ to $r\to\infty$,

$$\rho\int_R^\infty\left(\frac{\dot{F}}{r^2}-\frac{2F^2}{r^5}\right)dr=\int_R^\infty\left(-\frac{\partial p}{\partial r}+\frac{\partial \tau_{rr}}{\partial r}+\frac{3\tau_{rr}}{r}\right)dr, \tag{7}$$

where Eq. (1) has been used and ρ has been assumed constant (1000 kg/m^3) for $r>R$. The membrane at $r=a$ is assumed to have negligible thickness and therefore no mass. It is also assumed to exert a singular stress upon the fluid directed normal to its surface. Because this stress is singular, and because the material properties discontinuously change at the membrane, it is appropriate to split the integration operator on the right-hand side of Eq. (7) as

$$\int_R^\infty \Rightarrow \int_R^{a^-}+\int_{a^+}^\infty, \tag{8}$$

which upon integration yields

$$\rho\left(\frac{\dot{F}}{R}-\frac{1}{2}\frac{F^2}{R^4}\right)=p_R-p_{a^-}+p_{a^+}-p_\infty(t)+\tau_{rr}^{a^-}-\tau_{rr}^{a^+}-\tau_{rr}^{R}+\tau_{rr}^{\infty}+\int_R^{a-}\frac{3\tau_{rr}}{r}dr+\int_{a^+}^{\infty}\frac{3\tau_{rr}}{r}dr. \quad (9)$$

A force balance at the bubble surface $r=R$ yields

$$p_B=p_R+\frac{4\mu}{R}\dot{R}+\frac{2\sigma}{R}, \quad (10)$$

which is the usual expression relating bubble internal pressure p_B to the liquid pressure on the bubble surface p_R via the viscous and surface tension stresses. We neglect any vapor or gas exchange between the bubble and liquid so the bubble pressure is assumed to depend only on its volume according the usual polytropic relation

$$p_B=p_{B_0}\left(\frac{R_0}{R}\right)^{3\gamma}, \quad (11)$$

with $p_{B_0}=2\sigma/R_0+p_0$ being the equilibrium bubble pressure when $R=R_0$. The bubble volume change is fast, so we assume that it is effectively adiabatic before collapse and accordingly set $\gamma=1.4$. A force balance at $r=a$, corresponding to the usual one at $r=R$ quoted in Eq. (10), yields

$$-p_{a^-}+\tau_{rr}^{a^-}+\frac{2T(\lambda)}{a}=-p_{a^+}+\tau_{rr}^{a^+}, \quad (12)$$

where $T(\lambda)$ is the elastic tension in the membrane with stretch λ. The remaining integrals in Eq. (9) can be easily evaluated given Eqs. (5) and (6). Doing this, taking $\tau_{rr}^{\infty}=0$, applying Eqs. (10) and (12), neglecting elasticity of the liquid, and invoking $F=R^2\dot{R}$, yields

$$R\ddot{R}+\frac{3}{2}\dot{R}^2=\frac{1}{\rho}\left[p_B-p_\infty(t)-\frac{2\sigma}{R}-4\mu\frac{\dot{R}}{R}-\frac{2T(\lambda)}{a}-\frac{4}{3}\frac{G}{a^3}(R^3-R_0^3)-4(\mu_t-\mu)\frac{R^2\dot{R}}{a^3}\right]. \quad (13)$$

The final three terms of this expression are extensions to the standard Rayleigh–Plesset equation. In order of appearance in Eq. (13), they are the effects of the membrane tension, the elasticity beyond the membrane, and the viscosity jump across the membrane. We consider ranges of $T(\lambda)$, G, and μ_t for kidney tissue in Sec. (3).

So long as there is no significant liquid compressibility in the neighborhood of and beyond the membrane, which would be the case in our application, a similar modification can be made to compressible forms of the bubble dynamics equations, as done for a bubble in a weakly compressible viscoelastic medium by Yang and Church.[12] This, however, is not necessary here since we do not study collapse and rebound, the only cases where compressibility is expected to play a substantive role.

The membrane tension T in Eq. (13) is a function of stretch $\lambda=a/A$ [see Eq. (22)] and other terms in Eq. (13) depend on radius a, which changes according to the local velocity [Eq. (1)] as

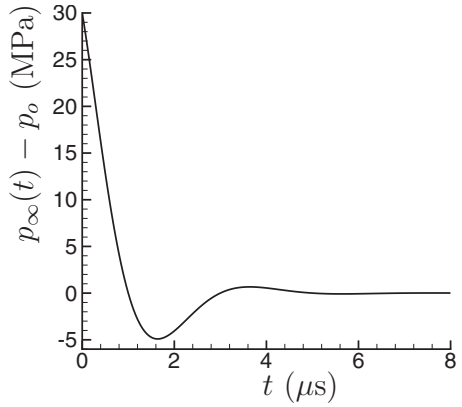

FIG. 2. Assumed lithotriptor shock profile: maximum of 30 MPa, minimum of −4.9 MPa.

$$\dot{a}=u[r=a(t),t]=\frac{R^2\dot{R}}{a^2}. \quad (14)$$

Equations (13) and (14) are solved with a stiff equation solver [LSODE (Ref. 17)] with initial conditions

$$R(0)=R_0, \quad \dot{R}(0)=0, \quad a(0)=A. \quad (15)$$

Results are relatively insensitive to R_0; we take $R_0=1$ μm for all cases. The initial membrane radius is taken to be $A=5$ μm, as appropriate for a small vessel.

B. Lithotriptor shock profile

The pressure field in a kidney of a shock from any particular lithotriptor is not precisely known and probably varies considerably depending on the various parameters of the configuration. It is thought to have a peak positive pressure, which abruptly rises to tens of megapascals, that is followed for about 2 μs by a negative pressure of $\lesssim$10 MPa. We assume a profile

$$p_\infty(t)=p_0+p_A e^{-t/\tau}\cos\left(\frac{\pi t}{2\tau}\right), \quad (16)$$

where $p_A=30$ MPa, $p_0=0.101$ MPa ($\approx$1 atm), and $\tau=1$ μs. This profile is plotted in Fig. 2. It resembles measured lithotriptor pressure histories.[18] The conclusions of this paper are independent of the details of the assumed shock profile.

III. MATERIAL PROPERTIES ESTIMATES

We assume that the bubble nuclei are in small blood vessels, and so we set viscosity $\mu=0.005$ Pa s, which is typical for microcirculation hematocrit values and high rates of strain.[19] Blood's surface tension under normal conditions is approximately $\sigma=0.06$ N/m.[20,21] The blood vessels in the kidney have a collagenous basement membrane with interstitial cells, extracellular material, and other vessels beyond that.[22] Mechanical properties of these materials are estimated in the following subsections.

A. Membrane constitutive model

Given the regular, tubular structure of kidney tissue (e.g., Jamison and Kriz[22]), we expect the membrane encasing

a bubble to have by far the largest influence on the bubble for two reasons. The first is simply proximity: the velocity and deformation fields of the bubble will decay as $1/r^2$ so the closest material will have dominant elastic influence. The second reason is that thin-walled shell-membrane structures are significantly more resistant to expansion from the inside than crushing from the outside, which causes them to buckle. Beyond the vessel we consider containing the bubble nucleus, which resists expansion, the nearby vessels in the kidney will be crushed and are therefore expected to be more fluidlike than elastic. There is cellular and extracellular matrix materials between the basement membranes, but it is thought[23,24] that basement membranes are the most important structural components of small vessels. We shall see in Sec. IV that even the highest estimate we can justify for the overall tissue elasticity is insufficient to significantly suppress cavitation.

The simplest way to proceed for modeling the elastic behavior of the membranes is simply by choosing Young's modulus, but like many biological materials the elasticity of basement membranes is significantly nonlinear. Welling *et al.*[24] reported that the effective modulus is $Y \approx 2-5$ MPa for small deformations, but $Y \approx 20$ MPa for large deformations. Since we need to track the entire range of deformations in our model, a more complete description is warranted.

Our constitutive model is constructed to reproduce the pressure-diameter data for the inflation of a renal tubule.[24] We start from well-known continuum mechanics results for membrane elasticity (e.g., Humphrey[25]) that relates the stress tensor $\mathbf{t}$ to a strain energy function W,

$$ht_{\alpha\beta} = \frac{2H}{J_{2D}} F_{\alpha\Sigma} F_{\beta\Delta} \frac{\partial W}{\partial C_{\Sigma\Delta}}, \tag{17}$$

where H is the initial predeformation thickness of the membrane of current thickness h so $F_{33}=\lambda_3=h/H$, $\mathbf{C}$ is the right Cauchy–Green tensor $\mathbf{C}=\mathbf{F}^T\cdot\mathbf{F}$, and $\mathbf{F}$ is the deformation gradient tensor. For a thin membrane the form of $\mathbf{F}$ is

$$\mathbf{F} = \begin{bmatrix} F_{11} & F_{12} & 0 \\ F_{21} & F_{22} & 0 \\ 0 & 0 & F_{33} \end{bmatrix}. \tag{18}$$

In principal coordinates, it is diagonal with the principal stretches on its diagonal: $\mathbf{F}=\mathrm{diag}[\lambda_1,\lambda_2,\lambda_3]$. In Eq. (17), the subscripted indexes α, β, Σ, and Δ each take values of only 1 or 2 reflecting the two-dimensional character of the membrane. J_{2D} in Eq. (17) is the determinant of the two-dimensional deformation gradient: $J_{2D}=F_{11}F_{22}-F_{12}F_{21}$.

We assume a simple strain energy function

$$W = W_0 e^{\alpha(I_C-3)}, \tag{19}$$

where $I_C=C_{11}+C_{22}+C_{33}$ is the first invariant of the Cauchy–Green tensor. In terms of principal stretches, it is $I_C=\lambda_1^2+\lambda_2^2+\lambda_3^2$. More general formulas than Eq. (19) might improve the apparent fit to the data, but pursuing this is unnecessary for our objectives and also probably unwarranted given that the data available for fitting are limited. The experiments were not designed with the intent to develop constitutive models, and so are missing some of the details (e.g., the stretch along the tubule) that would be needed to refine the constitutive model with confidence.

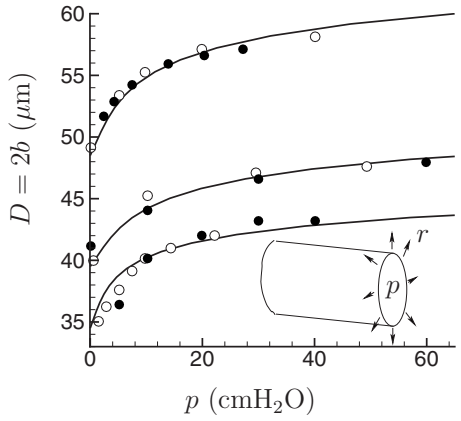

FIG. 3. Pressure-diameter relation for a renal tubule. The symbols show the data of Welling *et al.* (Ref. 24) for rabbit renal tubules. The (—) are from the effective stress of Eq. (21) with $\alpha=12$, $W_0=5000$ N/m^2, and $H=0.1$, 0.25, and 0.25 μm for the three sets of data shown. (The H were selected from the range reported (Ref. 24) to provide the best fit for constant B and α.)

For the inflation of the approximately cylindrical membrane of Welling *et al.*,[24] we assume that $\lambda_1=1$ and take $\lambda_2=\lambda=b/B$, where b and B are the radius and initial zero-stress radius, respectively. The axial boundary conditions are unclear from the experimental setup so the $\lambda_1=1$ assumption seems best for making our estimates. With this assumption, Eq. (17) using Eq. (19) yields azimuthal principal tension,

$$T_2 \equiv ht_{22} = \frac{2W_0\alpha H}{\lambda}\left(1-\frac{1}{\lambda^4}\right)e^{\alpha(\lambda^2+1/\lambda^2-2)}, \tag{20}$$

with corresponding pressure

$$p = \frac{T_2}{r} = \frac{T_2}{\lambda R}. \tag{21}$$

The fitted pressure-diameter curves are shown in Fig. 3 along with the experimental data.

For the spherical membrane inflation we consider in the current model, $\lambda_1=\lambda_2=\lambda=a/A$. where a is the radius and A is the initial radius of the sphere. In this case, both principal tensions are

$$T = 2W_0\alpha H\left(1-\frac{1}{\lambda^6}\right)e^{\alpha(2\lambda^2+1/\lambda^4-3)}, \tag{22}$$

with corresponding pressure

$$p_m = \frac{2T}{a}. \tag{23}$$

This pressure appears in Eq. (13). The membranes are observed to rupture for $\lambda \gtrsim 1.22$,[24] so we set $p_m=0$ when this occurs.

B. Bulk viscoelasticity

There are other components to renal tissue aside from basement membranes that we need to consider. We focus the present discussion on the inner medulla where injury is typically first observed.[8] The membranes of various capillary vessels and vasa recta, collecting ducts, and thin limbs of the

loops of Henle are lined with endothelial cells on their insides and surrounded by extracellular material with relatively low collagen content[26] and interstitial cells that bridge between them. As previously discussed,[3] none of these are expected to have any significant elasticity. Reported values of linear elastic moduli for cells are ~1 kPa, well less than that of basement membranes of 1–20 MPa.[24] Yang and Church[12] showed that elastic moduli of ~1 MPa for the entire material surrounding a bubble would suppress bubble growth for 1 MPa peak-to-peak, 1 MHz ultrasound. In the inner medulla, only the basement membranes are expected to have >1 MPa stiffness and they account for less than 1% of the volume of the overall tissue. Supporting this, Welling *et al.*[24] found no difference in the elasticity of renal tubule elasticity before and after the epithelial cells were chemically removed. However, with this type of reasoning, we would expect only $G \approx 1$ kPa for $r > a(t)$, but the tissue structure is complex and there are other measurements to consider.

Aside from the renal tubules, there are no detailed measurements of the microstructural material properties of renal tissue. So we must estimate the effective elastic response of the material surrounding the basement membrane based on bulk tissue measurements. Even for these studies, though, the deformations are either significantly slower than the ~10 μs expected for bubble expansion or deduced from ultrasound frequency shear wave dynamics, whose amplitude is small and whose deformation character is expected to be significantly different than that of an expanding bubble. Nevertheless, the available measurements allow us to establish bounds for making our estimates. Given the uncertainty of the data, we craft the discussion around linear elasticity moduli for our estimation purposes. The deformations are, of course, large, which would need to be more formally treated if data were available for crafting more precise models.

Basic stress-elongation data of Melvin *et al.*[27] suggest whole live organ linear elasticity with modulus $E \lesssim 2$ MPa. Measurements of sections of cortex tissue show this same stiffness, but only after 20%–30% strains are applied.[28] Before this level of deformation, the apparent modulus of elasticity appears to be <100 kPa.[29] This is consistent with the 20 Hz small strain (<2%) measurements of cortex tissue of Nasseri *et al.*,[29] which show $Y \approx 10$ kPa. Extrapolation of their data to the ~100 kHz expected for bubble growth still suggests $Y \lesssim 100$ kPa. Ultrasound measurements of other soft tissues also support these relatively low moduli. Experimental limitations of Firzzell *et al.*[30] set an upper bound of $Y < 1$ MPa for liver. Madsen *et al.*[31] fitted similar ultrasound data with a Voigt viscoelasticity model to suggest $Y \approx 10$ kPa. All these values will be considered in parametrizing the model in Sec. IV.

We also need estimates of the expected tissue viscosity for $r > a(t)$. Though only ultrasound measurements[30–32] reach the deformation rates expected in the neighborhood of a growing cavitation bubble, they are thought to yield relatively low values because the viscosity arises from dissipation at the macromolecular rather than cellular scale due to the short wavelength of the sound.[30] Ultrasound measurements at 1 MHz suggest a viscosity for liver of 0.15 Pa s,[32] which is about a factor of 10 higher than the viscosity predicted by fitting a Voigt model through 2–14 MHz ultrasound measurements for liver[31] or a Voigt-like model for 6–20 MHz ultrasound measurements for kidney.[33] It is possible that the longer sound wavelength at 1 MHz causes more cell-scale deformations leading to higher viscosity. The deformation caused by bubble expansion will be larger than cell scale, and so we expect the ultrasound measurements to provide a lower bound on viscosity, with significantly more viscous resistance possible. Mechanical testing of kidneys and most soft tissues at 20 Hz suggest much higher viscosities: Nasseri *et al.*[29] reported ~100 Pa s for sections of kidney cortex. Extrapolation with their power law fit to 100 kHz suggests 0.15 Pa s.

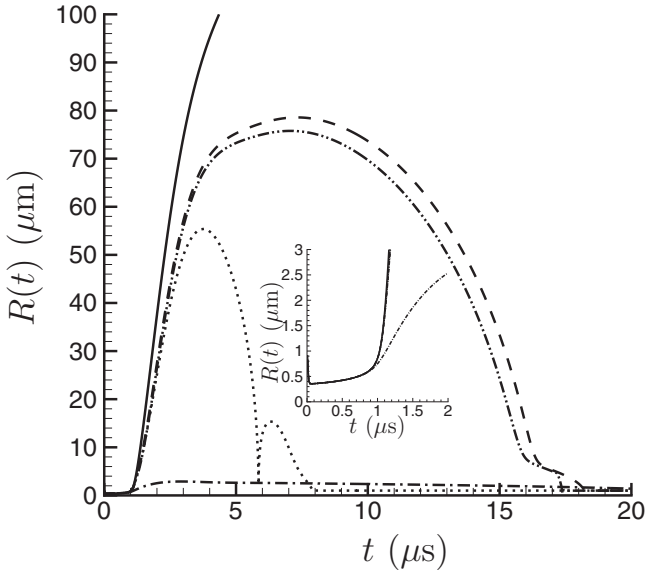

FIG. 4. Bubble radius evolution: (—) $Y=0$, $f_t=0$, $\mu_t=0$; (- - - -) $Y=10$ kPa, $f_t=1$, $\mu_t=0.15$ Pa s; (–··–) $Y=10$ kPa, $f_t=100$, $\mu_t=0.15$ Pa s; (·····) $Y=1$ MPa, $f_t=1$, $\mu_t=0.15$ Pa s; (–·–) $Y=10$ kPa, $f_t=1$, $\mu_t=15.0$ Pa s.

IV. MODEL PREDICTIONS

We consider five cases, the results of all of which are shown in Fig. 4. The first is a baseline unconfined Rayleigh–Plesset solution, which corresponds to $A \to \infty$. This is shown as the solid line in the figure. As expected, the bubble grows to be well over $R=100$ μm radius in this case. For cases with a membrane ($A=5$ μm) and elastic tissue beyond, the eventual size of the bubble and membrane cannot be regarded as quantitatively relevant unless it is substantially suppressed in its growth. If it grows large, it will exceed the yielding or tearing thresholds of the materials, which would be even more challenging to make reliable estimates for. Thus, our main conclusions will be concerning whether or not the bubble grows large and not its eventual size *per se*.

For the second case, we consider the least confining constitutive properties from the discussions in Sec. III. We thus take the membrane dynamics as modeled in Sec. III A, Young's modulus in $r > a$ to be $Y=10$ kPa as suggested for relatively small deformation[29] and by ultrasound,[31] and the tissue viscosity of 0.15 Pa s as suggested from ultrasound[32] and extrapolation from low frequencies.[29] This confinement

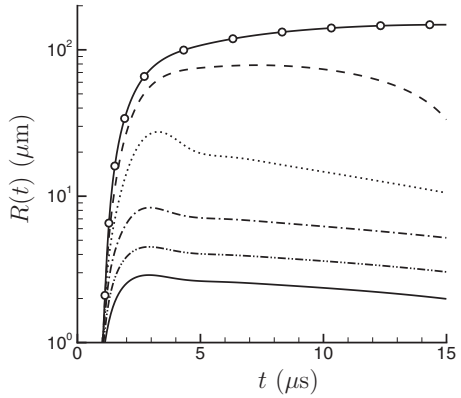

FIG. 5. Bubble radius evolution for (−∘−) $Y=0$, $f_t=0$, $\mu_t=0$, and $Y=10$ kPa, $f_t=1$, with viscosities (- - - -) $\mu_t=0.15$ Pa s, (·····) $\mu_t=0.47$ Pa s, (−·−) $\mu_t=1.5$ Pa s, (−··−) $\mu_t=4.7$ Pa s, and (——) $\mu_t=15$ Pa s.

does suppress the bubble growth somewhat, though it still grows to a radius of nearly $R\approx 80$ μm, far exceeding any expectations of the yield strain for the membrane and surrounding tissue.

For the final three cases, we in turn increase membrane elasticity $T(\lambda)$, G, and μ_t by factors of 100. This brings their properties into the high end of the ranges estimated in Sec. III. Though it is expected to be the stiffest component of the tissue, increasing the stiffness of the basement membrane model by a factor $f_T=100$ (i.e., $T'=f_T T$) does little to additionally constrain the bubble. As seen in the figure, it only reduces the maximum radius by only a few micrometers. More surprisingly, increasing the elastic modulus of the exterior material by a factor of 100 to 1 MPa, bringing it into the range expected for the largest deformations at the slowest rates,[29] still does not suppress bubble growth. The maximum radius is still more than 50 μm as seen in the figure, and the material would be expected to yield well before this point. This level of exterior elasticity was sufficient to suppress bubble growth in the ultrasound experiments and simulations of Caskey *et al.*,[34] which have weaker forcing, but it is not clear that such a high level of elasticity is justified, at least not for the whole range of deformation. Tissue viscosity was also neglected in that study. Here, we find that tissue viscosity is actually the most effective restriction of bubble growth. Increasing μ_t to 15 Pa s, which is well within the range measured for tissues by methods other than by ultrasound, significantly suppresses the growth. For this tissue viscosity, the membrane would not be expected to rupture. Plots for several viscosities are shown in Fig. 5.

The differences in the behavior of the different cases come from the expansion and do not significantly involve the bubble collapse, as can be seen from the inset in Fig. 4. When the bubble is small, changes in its size have little effect on the membrane and the viscoelastic tissue beyond because of the R^2/a^2 relation in displacements and velocities. For fixed bubble size, larger membranes (larger A) would also be significantly less confining for the same reason.

V. CONCLUSIONS AND ADDITIONAL DISCUSSION

The first principal conclusion of these model simulations is clear: the measured elasticity of a renal basement membrane is of itself far too weak to significantly alter the growth of a cavitation bubble confined within it, at least for a lithotriptor pressure pulse with $P_-\approx 5$ MPa. A spherical confinement model was employed for analytical simplicity, but the effect of the membrane elasticity on the bubble is so small that it does not seem possible that a cylindrical membrane would offer any significant confinement either. We show that the elasticity of the tissue beyond the membrane would also need to exceed all reported measurements for kidney tissue in order to avoid large, presumably tearing strains. Given these predictions for elastic confinement, we are left to address what suppresses cavitation and injury in shock-wave lithotripsy, at least for the first 1000 or so shocks. A possible explanations is that there are insufficient cavitation nuclei in the tissue so other mechanisms such a shear[3,4] are needed to initiate injury. We cannot make an assessment of the normal density of cavitation nuclei here, but our estimates indicate that any confining effects on bubble dynamics are more likely to come via viscosity than elasticity. The largest reported elastic moduli for kidney tissue at any deformation rates do not substantially suppress bubble growth in our model. The largest viscosities, however, easily do, and even the smallest values reported, those that come from ultrasound measurements, have a significant suppressing effect on the maximum size reached by a bubble. The second principal conclusion is, therefore, that any tissue confinement of lithotriptor-shocked bubbles will most likely derive from tissue viscosity. It is well known that sufficient viscosity will suppress any motion, as has been specifically discussed for lithotriptor driven bubbles by Church;[35] our estimates suggest that tissues might have sufficient viscosity to suppress bubbles in small vessels. We can go on to speculate that it might be a slow reduction of tissue viscosity that eventually facilitates the more widespread injuries observed after ~1000 shocks are delivered. Pooling of blood in lesions, whatever their cause, is potentially a route to reduced viscous confinement. Similarly, examination of kidney tissue injured by shock-wave lithotripsy shows that the entire microstructure is disrupted,[36] which will also tend to reduce its viscosity and thereby perhaps also facilitate bubble growth and spreading cavitation damage.

ACKNOWLEDGMENTS

The author is grateful for fruitful discussions with M. Bailey about shock-wave lithotripsy and bubble confinement in tissue. This work was partially supported by NIH Grant No. PO1-DK043881.

APPENDIX: AXIAL PRESSURE RELEASE ESTIMATES IN ELASTIC CYLINDERS

This appendix serves as supplemental justification of the relevance of the spherical confinement for the more realistic, but more analytically challenging, case of cylindrical confinement. The strongest argument in this regard, however, remains the fact that the bubble is not substantively confined

by the spherical membrane, which is in a sense maximally confining. If the spherical membrane does not suppress expansion, we cannot expect a more realistic cylindrical membrane to either.

We make estimates in two limits of how quickly flow along the vessel would release confinement in the neighborhood of the bubble. In one limit, the pressure is countered by inertia along the tubule and in the other the pressure is countered by viscous forces in the tubule. For making some of our estimates, it will be simpler to revert to a linear elasticity model. In this case we take $T=T_y(\lambda-1)$ and use $T_y=0.16$ N/m as in a previous effort.[3]

1. Inertia mediated pressure release

Elastic fluid filled cylindrical membranes are known to support waves, the pulse wave in the arterial system being the most celebrated, and the speed of this wave governs the rate of pressure release along the vessel. For small amplitudes, the speed of such waves is[37]

$$c=\sqrt{\frac{T}{2\rho r_0}}, \tag{A1}$$

where T is the elastic tension modulus and r_0 is the undeformed radius of the tubule. For $T=0.16$ N/m and $r_0=5$ μm, this wave speed is 4 m/s so it takes 2.5 μs to travel the distance of the tubule's diameter $(2r_0)$. This is comparable to the time scale of the bubble growth to the point at which it would stretch the membrane to the breaking point, so we do not expect an inertia based mechanism of this sort to play a dominant role in releasing the excess membrane induced pressure in the neighborhood of the bubble. This analysis neglects the mass of any attached surrounding tissue, but this would serve only to slow the wave speed. However, for inertia to be the dominant mechanism, the Reynolds number of the system should be large. The velocity depends on the bubble dynamics, but is slower than the wave speed, which we therefore use to establish an upper bound on the Reynolds number: $\mathrm{Re}=\rho c r_0/\mu=4$. This is too low to expect a purely inertial behavior, so we also make an estimate in the viscous limit.

2. Viscosity mediated pressure release

In this case, a similar set of quasi-one-dimensional assumptions to those used[37] in is establishing the elastic tube wave speed is used in the viscous limit. To this end, the flow is assumed to be one dimensional and to have the well-known Poiseuille parabolic velocity profile for which the volumetric flow rate q is related to the pressure drop Δp along a tubule segment length ℓ by

$$q=\frac{\pi r^4 \Delta p}{8\mu\ell}. \tag{A2}$$

In the limit of an infinitesimal tube segment length $\ell\to dx$,

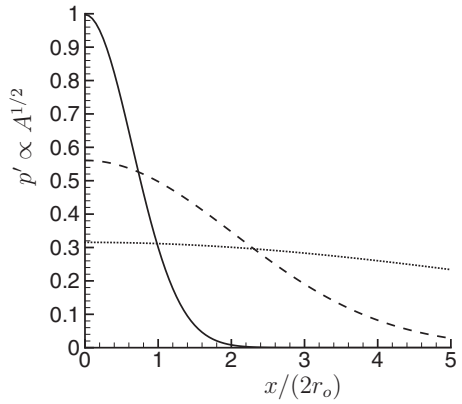

FIG. 6. Estimated pressure distribution for a viscous mediated pressure release along a flexible cylindrical membrane (see text) at times of (—-) 1 μs, (- - - -) 10 μs, and (·····) 100 μs.

$$q=-\frac{\pi r^4}{8\mu}\frac{\partial p}{\partial x}. \tag{A3}$$

This is a consequence of conservation of momentum. A differential form of conservation of mass, again assuming one-dimensional flow with volume flux q, is

$$\frac{\partial A}{\partial t}+\frac{\partial q}{\partial x}=0, \tag{A4}$$

where A is the fluid-filled area of the tube. Assuming linear elasticity, as appropriate for our estimates which are made in the small deformation limit, the internal pressure in Eq. (A3) is related to the tube radius by

$$p-p_0=\frac{\tau}{r}=T\left(\frac{1}{r_0}-\frac{1}{r}\right). \tag{A5}$$

Substituting this into Eq. (A3) and the result into Eq. (A4) yields a differential equation for the tube's area

$$\frac{\partial A}{\partial t}-\frac{\partial}{\partial x}\left(\alpha A^{1/2}\frac{\partial A}{\partial x}\right)=0, \tag{A6}$$

where

$$\alpha=\frac{T}{16\pi^{1/2}\mu}. \tag{A7}$$

Small perturbations A' to initial undeformed area A_0 evolve according to

$$\frac{\partial A'}{\partial t}-\beta\frac{\partial^2 A'}{\partial x^2}=0, \tag{A8}$$

where $\beta=A_0^{1/2}\alpha$. Plotting $p'\propto\sqrt{A'}$ for the fundamental solution of this equation [initial condition $A'(x,t=0)=\delta(x)$] in Fig. 6 with $T=0.16$ N/m shows that the pressure should also slowly spread relative to the bubble growth by this viscous mechanism.

[1]M. R. Bailey, L. A. Crum, A. P. Evan, J. A. McAteer, J. C. Williams, Jr., O. A. Sapozhnikov, R. O. Cleveland, and T. Colonius, "Cavitation in shock wave lithotripsy," in *The Fifth International Symposium on Cavitation*, Osaka, Japan, November 2003, Paper No. Cav03 OS-2-1-006.
[2]A. P. Evan, L. R. Willis, J. E. Lingeman, and J. A. McAteer, "Renal trauma and the risk of long-term complications in shock wave lithotripsy,"

Nephron **78**, 1–8 (1998).
[3]J. B. Freund, T. Colonius, and A. P. Evan, "A cumulative shear mechanism for tissue damage initiation in shock-wave lithotripsy," Ultrasound Med. Biol. **33**, 1495–1503 (2007).
[4]M. Lokhandwalla, J. A. McAteer, J. C. Williams, Jr., and B. Sturtevant, "Mechanical haemolysis in shock wave lithotripsy (SWL): II. *In vitro* cell lysis due to shear," Phys. Med. Biol. **46**, 1245–1264 (2001).
[5]D. Dalecki, C. H. Raeman, S. Z. Child, D. P. Penney, R. Mayer, and E. L. Carstensen, "The influence of contrast agents on hemorrhage produced by lithotripter fields," Ultrasound Med. Biol. **23**, 1435–1439 (1997).
[6]P. Zhong, I. Cioanta, S. Zhu, F. H. Cocks, and G. M. Perminger, "Effects of tissue constraint on shock wave-induced bubble expansion *in vivo*," J. Acoust. Soc. Am. **104**, 3126–3129 (1998).
[7]P. Zhong, Y. Zhou, and S. Zhu, "Dynamics of bubble oscillations in constrained media and mechanisms of vessel rupture in SWL," Ultrasound Med. Biol. **27**, 119–134 (2001).
[8]P. M. Blomgren, B. A. Connors, J. E. Lingeman, L. R. Willis, and A. P. Evan, "Quantitation of shock wave lithotripsy-induced lesion in small and large pig kidneys," Anat. Rec. **249**, 341–348 (1997).
[9]J. Cui, M. F. Hamilton, P. S. Wilson, and E. A. Zabolotskaya, "Bubble pulsations between parallel plates," J. Acoust. Soc. Am. **119**, 2067–2072 (2006).
[10]J. S. Allen and R. A. Roy, "Dynamics of gas bubbles in viscoelastic fluids. II. Nonlinear viscoelasticity," J. Acoust. Soc. Am. **108**, 1640–1650 (2000).
[11]S. Y. Emelianov, M. F. Hamilton, Y. A. Ilinskii, and E. A. Zabolotskaya, "Nonlinear dynamics of a gas bubble in an incompressible elastic medium," J. Acoust. Soc. Am. **115**, 581–588 (2004).
[12]X. Yang and C. C. Church, "A model for the dynamics of gas bubbles in soft tissue," J. Acoust. Soc. Am. **118**, 3595–3606 (2005).
[13]C. C. Church and X. Yang, "A theoretical study of gas bubble dynamics in tissue," in *Proceedings of the 17th International Symposium on Nonlinear Acoustics*, edited by A. A. Atchley, V. W. Sparrow, and R. M. Keolian (American Institute of Physics, Melville, 2006), pp. 217–224.
[14]T. Ye and J. L. Bull, "Microbubble expansions in a flexible tube," J. Biomed. Eng. **128**, 554–563 (2006).
[15]T. Ye and J. L. Bull, "Direct numerical simulations of micro-bubble expansion in gas embolotherapy," J. Biomed. Eng. **126**, 746–759 (2004).
[16]A. Prosperetti, "A generalization of the Rayleigh–Plesset equation of bubble dynamics," Phys. Fluids **25**, 409–410 (1982).
[17]A. Hindmarsh, "LSODE. Ordinary differential equation system solver," Lawrence Livermore National Laboratory, Technical Report No. ESTSC–000216CY0MP00, 1983.
[18]R. O. Cleveland, M. R. Bailey, N. Fineberg, B. Hartenbaum, M. Lokhandwalla, G. A. McAteer, and B. Sturtevant, "Design and characterization of a research electrohydraulic lithotripter patterned after the Dornier HM3," Rev. Sci. Instrum. **71**, 2514–2525 (2000).
[19]R. L. Whitmore, *Rheology of the Circulation* (Pergamon, Oxford, 1968).
[20]E. Hrncir and J. Rosina, "Surface tension of blood," Physiol. Res. **46**, 319–321 (1997).
[21]J. Rosina, E. Kvasnak, D. Suta, H. Kolarova, J. Malek, and L. Krajci, "Temperature dependence of blood surface tension," Physiol. Res. **56** (Supplement 1), S93–S98 (2007).
[22]R. L. Jamison and W. Kriz, *Urinary concentrating mechanism: structure and function* (Oxford University Press, New York, 1982).
[23]J. B. West, K. Tsukimoto, O. Mathieu-Costello, and R. Prediletto, "Stress failure in pulmonary capillaries," J. Appl. Physiol. **40**, 1731–1742 (1991).
[24]L. W. Welling, M. T. Zupka, and D. J. Welling, "Mechanical properties of basement-membrane," News Physiol. Sci. **10**, 30–35 (1995).
[25]J. D. Humphrey, *Cardiovascular Solid Mechanics: Cells, Tissues, and Organs* (Springer, New York, 2002).
[26]L. Osvaldo and H. Latta, "Interstitial cells and the renal medulla," J. Ultrastruct. Res. **15**, 589–613 (1966).
[27]J. W. Melvin, R. L. Stalnaker, and V. L. Roberts, "Impact injury mechanisms in abdominal organs," Proceedings of the 17th Stapp Car Crash Conference, SAE Trans. 730968, 115–126 (1973).
[28]M. Farshad, M. Barbezat, P. Flüeler, F. Schmidlin, P. Graber, and P. Niederer, "Material characterization of the pig kidney in relation with the biomechanical analysis of renal trauma," J. Biomech. **32**, 417–425 (1999).
[29]S. Nasseri, L. E. Bilston, and N. Phan-Thien, "Viscoelastic properties of pig kidney in shear, experimental results and modelling," Rheol. Acta **41**, 180–192 (2002).
[30]L. A. Frizzell, E. L. Carstensen, and J. F. Dyro, "Shear properties of mammalian tissues at low megahertz frequencies," J. Acoust. Soc. Am. **60**, 1409–1411 (1977).
[31]E. L. Madsen, H. J. Sathoff, and J. A. Zagzebski, "Ultrasonic shear wave properties of soft tissues and tissue like materials," J. Acoust. Soc. Am. **74**, 1346–1355 (1983).
[32]S. Girnyk, A. Barannik, E. Barannik, V. Tovstiak, A. Marusenko, and V. Volokhov, "The estimation of elasticity and viscosity of soft tissues in vitro using the data of remote acoustic palpation," Ultrasound Med. Biol. **32**, 211–219 (2006).
[33]X. Yang and C. C. Church, "A simple viscoelastic model for soft tissues in the frequency range 6-20 MHz," IEEE Trans. Ultrason. Ferroelectr. Freq. Control **53**, 1404–1411 (2006).
[34]C. F. Caskey, S. M. Stieger, S. Qin, P. A. Dayton, and K. W. Ferrara, "Direct observations of ultrasound microbubble contrast agent interaction with the microvessel wall," J. Acoust. Soc. Am. **122**, 1191–1200 (2007).
[35]C. C. Church, "A theoretical study of cavitation generated by an extracorporeal shock wave lithotripter," J. Acoust. Soc. Am. **86**, 215–227 (1989).
[36]Y. Shao, B. A. Connors, A. P. Evan, L. R. Willis, D. A. Lifshitz, and J. E. Lingeman, "Morphological changes induced in the pig kidney by extracorporeal shock wave lithotripsy," Anat. Rec. **275A**, 979–989 (2003).
[37]J. Lighthill, *Mathematical Biofluiddynamics* (Society for Industrial and Applied Mathematics, Philadelphia, 1989).